RSC Applied Polymers

PAPER

View Article Online
View Journal

Cite this: DOI: 10.1039/d6lp00005c

Toward sustainable SLA 3D printing: glycerol-based 1,3-diether-2-methacrylates with solvent capability for *in situ* polymer blend formation

Zahra Sekhavat Pour, Pravin S. Shinde, Jun Wang, Mustapha Iddrisu, Tibor Szilvási and Jason E. Bara *

Development of sustainable and environmentally friendly stereolithography (SLA) 3D printing resins has gained considerable attention in recent years. Towards this goal, we have successfully employed glycerol-based 1,3-diether-2-methacrylate monomers that offer tunable mechanical and thermal properties. These monomers also act as solvents for thermoplastics such as polystyrene (PS) and poly(methyl-methacrylate) PMMA. This dual functionality enables the direct fabrication of polymer blends using only a consumer-level SLA 3D printer. The resulting blends exhibit composition-dependent phase morphologies that significantly influence mechanical properties. For instance, incorporating 5 wt% waste PS (wPS) results in complete phase separation with a stratified morphology in each layer and substantially diminished elongation at break, whereas 10 wt% wPS led to a more uniform dispersion and improved mechanical behavior. In contrast, PMMA-containing systems provide more transparent blends and continuous matrix morphology without compromising elasticity. Thermal analysis revealed the presence of two distinct glass transition temperatures (T_g) corresponding to the matrix formed *via* monomer curing and the thermoplastic phase, confirming the immiscibility of the blends. However, shifts and broadening of T_g values indicate improved interfacial interactions across the studied composition range. These results highlight the potential of glycerol-based methacrylate monomers as multifunctional platforms for tunable resin formulations and sustainable SLA 3D printing.

Received 5th January 2026,
Accepted 17th February 2026

DOI: 10.1039/d6lp00005c

rsc.li/rscapplpolym

1. Introduction

Glycerol (also known as glycerin, 1,2,3-propanetriol, *etc.*) has transitioned from being a critical industrial chemical in limited supply to an abundant by-product of biodiesel production over the past seven decades. Global biodiesel production was projected to reach 41.4 × 10^9 L by 2025, a 33% increase from 2015.[1,2] Since ~10% of the weight of biodiesel is generated as glycerol, a significant amount of waste glycerol has been produced. Therefore, the reuse and valorization of glycerol have become urgent priorities.[3] Numerous catalytic strategies, including oxidation, etherification, esterification, and acetalization, have been explored to convert glycerol into value-added chemicals, such as organic acids, diols, and fuels.[4–10]

The three hydroxyl (-OH) groups of glycerol make it an excellent precursor for multifunctional monomers and biobased polymers. Its non-flammability, low volatility, and low toxicity further enhance its suitability as a sustainable feedstock.[11,12] Glycerol and its derivatives have been used in polycondensation polymerization to produce materials such as polyglycerols, bio-polyesters, and multifunctional polyurethanes with properties like self-healing and shape recovery.[13,14] However, most reported glycerol polycondensates remain limited to oligomeric or crosslinked structures and often require complex synthesis steps, which hinder broader commercial adoption.[15]

Radical polymerization has also been utilized in the synthesis of glycerol-derived polymers.[16–18] Methods such as (trans)esterification[19] or transvinylation[20] are typically employed to functionalize glycerol with (meth)acrylic, vinylic, or allylic groups. Such biobased monomers are compatible with various radical polymerization methods and have enabled the synthesis of high-performance thermoplastics and adhesives. For instance, esterifying crude glycerol with acrylic acid, followed by RAFT polymerization to mitigate gelation, has resulted in the production of glycerol-based thermoplastics with high molecular weights and performance comparable to conventional wood adhesives.[15] Glycerol ketal(meth)acrylate monomers are synthesized by the reaction of various glycerol

Department of Chemical & Biological Engineering, The University of Alabama, Tuscaloosa, AL, 35487-0203 USA. E-mail: jbara@eng.ua.edu

ketals and methyl(meth)acrylate *via* enzymatic transesterification and used to develop novel biopolymers with potential application in hard block polymers and adhesives.[21] The results of this study demonstrate how the choice of (meth)acrylate backbone and pendant side chain groups can be used to influence the thermal and rheological properties of the resulting polymers.

3D printing, also known as additive manufacturing (AM), is a transformative technology that builds complex three-dimensional objects layer by layer from digital models, enabling geometries that are difficult or impossible to achieve with traditional methods.[22] The global market for 3D printing materials has experienced exponential growth over the past decade, with photopolymers now accounting for nearly half of global material sales.[23] The global revenues for AM materials are expected to reach $30 B by 2032, with the largest market shares for the aerospace, defense, medical, and dental industries.[24] Stereolithography (SLA) is a well-established AM technique that enables the layer-by-layer photopolymerization of liquid resins into high-resolution parts with fast production times. Although it is an efficient and low-waste production method, the lack of sustainable resins for vat photopolymerization remains a major limitation, underscoring the need for environmentally friendly alternatives to support broader adoption.[25]

In recent years, there has been interest in the formulation and application of resins derived from renewable feedstocks such as lignin and vegetable oils.[26–28] For example, soybean oil methacrylates have been formulated into printable resins that showed full layer fusion, high print quality, and tunable mechanical properties, including stiffness and toughness, by varying their chemical composition and functionality.[29] Another renewable soybean oil-based epoxidized acrylate has also been processed by 3D laser printing to produce porous, biocompatible scaffolds capable of supporting human bone marrow stem cell growth.[30] Five 3D-printable, self-healing, reprocessable, and chemically degradable thermoset polymers were fabricated by the functionalization of different Jeffamines with vanillin methacrylate and formulated with vanillin acrylate to allow for printability. The resulting thermosets exhibited a broad range of mechanical properties (Young's modulus: 2.05–332 MPa), enabling diverse applications.[31] However, considerable efforts are still needed to develop environmentally friendly materials for SLA 3D printing that can replace commercial fossil fuel-based resins.

We previously reported the controlled synthesis of symmetric and non-symmetric 1,3-diether-2-propanol and 1,2,3-triether derivatives, starting from epichlorohydrin (ECH), a key molecule that can be obtained from glycerol *via* reaction with two equivalents of HCl.[8,32–34] While 1,2,3-triether compounds show excellent promise as tunable solvents, particularly for CO_2 absorption,[33] 1,3-diether-2-propanol serves as a versatile intermediate for synthesizing various functional molecules, including esters, ketones, and amines.[32,34–37] We recently utilized 1,3-diether-2-propanol compounds as precursors to synthesize UV-curable glycerol-based methacrylate monomers designed to serve as critical components in SLA 3D printing resins. Comprehensive evaluations of the thermal and mechanical properties of the 3D-printed objects were performed and reported in our recently published paper,[38] revealing that these straightforward monomers can create parts indistinguishable in appearance from highly optimized commercial resins. The versatility of these methacrylate monomers extends beyond their role in 3D printing resins. They can also function as solvents for certain commodity thermoplastics, effectively dissolving polystyrene (PS) and poly(methyl methacrylate) PMMA. This dissolved plastic is integrated into the printed structures, enabling the customization of their material properties, including mechanical properties. Therefore, these glycerol-based methacrylate monomers open new opportunities for creating polymer blends through SLA 3D printing. While polymer blends are commonly achieved through melt blending using equipment like extruders, the dual functionality of MAA-DEP as both a monomer and a solvent offers an innovative alternative for preparing polymer blends through a fundamentally distinct method.

Incorporation of non-reactive polymers or prepolymers into photopolymerizable monomers is a strategy to generate phase-separated structures through photopolymerization-induced phase separation.[39–41] In these systems, an initially homogeneous mixture becomes thermodynamically unstable as polymerization proceeds, owing to increasing molecular weight, reduced entropy of mixing, and rising viscosity of the forming network. As a result, the dissolved polymer or prepolymer demixes from the growing photopolymer matrix, producing composition-dependent phase morphologies. This behavior has been widely reported in UV-curable coatings, films, and bulk photopolymer systems containing dissolved polymers or oligomeric modifiers, where phase separation and domain size are governed by additive loading, molecular weight, and curing kinetics, and exploited to tailor optical, mechanical, and thermal properties.[42,43] This phenomenon has been rarely reported in the context of vat photopolymerization and SLA resin design; however, extending this concept to SLA printing enables composition-dependent control of microstructure and properties within printed objects.

In this work, we demonstrate how dissolving PS and PMMA into glycerol-based diether-methacrylate monomers significantly impacts the microstructure of the resulting polymer blends, thereby influencing their mechanical and thermal properties. Moreover, PS is a major contributor to plastic waste streams and is notoriously difficult to recycle by conventional means[44] such that incorporating materials like waste PS (wPS), PMMA, and potentially other thermoplastics into 3D printing resins provides a promising upcycling route that transforms discarded plastics into higher-value materials and proportionally reduces the volume of SLA resin required. By blending renewable glycerol-derived monomers with wPS and PMMA, this work demonstrates a circular materials design strategy in which bio-based feedstocks and waste plastics are combined to create sustainable resins for AM applications.

2. Experimental

2.1. Materials

(±)-ECH (99%) and 2-methoxyethanol (99%) were purchased from Beantown Chemical. ACS-grade ethanol (EtOH), methanol (MeOH), chloroform ($CHCl_3$), and sodium hydroxide (NaOH, 97%) were received from VWR, while methacrylic anhydride (MAA, 94%) was purchased from Sigma-Aldrich. 4-(Dimethylamino)pyridine (DMAP) was acquired from Chem-Impex International, and phenylbis(2,4,6-trimethylbenzoyl) phosphine oxide (BAPO), used as the initiator, was obtained from TCI America. Triethylamine (Et_3N) was purchased from Macron Fine Chemicals. wPS was obtained from food containers marked with resin identification code (RIC) 6. These containers were manually cut into small flakes (0.5–1.0 cm), washed with deionized water and EtOH, and dried in a vacuum oven at 60 °C overnight before use. The weight-average molecular weight (M_w) of wPS was determined to be 174.7 kDa using gel permeation chromatography (GPC).[45] Virgin PS (PS (45k): M_w = 45 kDa) and PMMA (M_w = 15 kDa) were purchased from Scientific Polymer Products (Ontario, NY, USA).

2.2. Synthesis of symmetric 1,3-diethers

Symmetric 1,3-diether-2-propanol compounds, including 1,3-diethoxypropan-2-ol (DEP), 1,3-dibutoxypropan-2-ol (DBP), and 1,3-bis(2-methoxyethoxy)propan-2-ol (DMEP), were synthesized from ECH and the corresponding alcohols following the method outlined in our previous studies.[2,34]

2.3. Synthesis of symmetric 1,3-diether-2-methacrylates

Three glycerol-based monomers, 1,3-diethoxypropan-2-yl methacrylate (MAA-DEP), 1,3-dibutoxypropan-2-yl methacrylate (MAA-DBP), and 2,5,9,12-tetraoxatridecan-7-yl methacrylate (MAA-DMEP), were synthesized through the reaction of the corresponding symmetric 1,3-diether-2-propanol compounds with MAA, using Et_3N and DMAP as catalysts (Scheme S1). The synthetic procedure followed the strategy previously reported in our earlier publication,[38] and is briefly summarized in the SI. Fig. 1 illustrates the chemical structures of the 1,3-diether-2-methacrylate monomers.

2.4. Resin formulation for 3D printing

To prepare the PS or PMMA solutions with symmetric 1,3-diether-2-methacrylate monomers, a specific amount of wPS (5 and 10 wt%), PS(45k) (10 wt%) or PMMA (5 and 10 wt%) was weighed and added to the monomer. The mixture was heated at 45 °C while stirring for a minimum of 5 h to obtain a clear solution. SLA 3D printing resins were formulated by incorporating 2.5 wt% BAPO photoinitiator into each PS or PMMA monomer solution. The mixtures were stirred for 10 min until a clear solution was achieved.

2.5. SLA 3D printing

3D printing was performed using an Elegoo Mars 4 MSLA printer (China) equipped with a 405 nm light source. Each layer with a thickness of 50 μm was exposed for 40 s for pure monomers and 50 s for PS or PMMA/monomer solutions. After printing, the 3D-printed parts were cleaned to remove any residual monomer, and finally, the parts were post-cured in a UV oven (Elegoo Mercury Plus) for an additional 10 min.

2.6. Characterization

^{1}H NMR spectra were acquired using a 500 MHz Bruker Avance instrument (Billerica, MA, USA). The viscosity of PS or PMMA solution was measured at 25 °C using an Anton Paar ViscoQC 300-L rotational viscometer equipped with a CP40 cone plate spindle. Glass transition temperature (T_g) values of the polymers were determined by differential scanning calorimetry (DSC) using a TA Instruments DSC Q20 (New Castle, DE, USA). 3D-printed samples were heated and cooled from −40 to 150 °C at a scan rate of 10 °C min^{-1} under a nitrogen atmosphere. Multiple heating and cooling cycles were performed to ensure reliable results.

Thermogravimetric Analysis (TGA) measurements were conducted using a SETARAM Labsys Evo thermal analyzer (KEP Technologies, TX, USA). An appropriate amount of 3D-printed polymer sample was placed in alumina (Al_2O_3) pans and heated from 25 to 700 °C at a heating rate of 10 °C min^{-1} under a constant flow of ultra-high purity argon gas (AR UHP300, Airgas). Tensile tests were performed using a compact table-top electromechanical-driven single-column load-frame universal testing machine (Test Resources Inc, Shakopee, MN, USA) equipped with a 1.1 kN load cell. Tests were conducted according to ASTM D 638 standards on specimens with dimensions of 82 mm × 12 mm × 2 mm. Degree of Conversion (DC) was determined using Fourier Transform Infrared Spectroscopy (FTIR) with a PerkinElmer Spectrum Two ATR-FTIR instrument. DC was calculated based on the change in the absorption intensity of the methacrylate C=C stretching vibration at 1638 cm^{-1} before and after 3D printing,

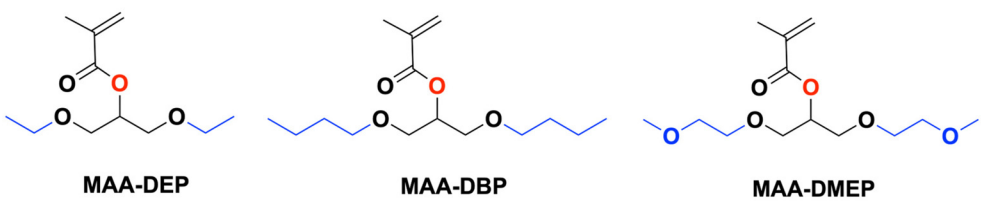

Fig. 1 Molecular structures of 1,3-diether-2-methacrylate monomers used in this work.

using the C=O stretching vibration (1715–1725 cm^{-1}) as an internal standard. Eqn (1) was used to calculate DC:

$$DC\,(\%) = \left(1 - \left(\frac{\left(\frac{A_{CC}}{A_{CO}}\right)_{Polymer}}{\left(\frac{A_{CC}}{A_{CO}}\right)_{Monomer}}\right)\right) \times 100 \qquad (1)$$

where $A_{C=C}$ represents the absorbance at 1638 cm^{-1} before and after 3D printing, while $A_{C=O}$ refers to the absorbance peak around 1715–1725 cm^{-1} in the monomer and polymer.[46,47]

The morphology of 3D-printed samples prepared from solutions of PS or PMMA in 1,3-diether-2-methacrylates was analyzed using a Thermo Fisher Scientific Apreo 2 SEM. Samples were cryogenically fractured in liquid nitrogen, coated with silver, and analyzed at an accelerating voltage of 5 kV. XRD measurements were performed using a Panalytical MPD X'pert Pro diffractometer (model: PW3050/60).

3. Results and discussion

3.1. Polymer blend formation through SLA 3D printing

This study explores a novel approach to polymer blend formation using SLA 3D printing. We previously reported the efficient synthesis of 1,3-diether-2-methacrylate monomers *via* Steglich esterification of glycerol-derived 1,3-diether-2-propanol with MAA, catalyzed by DMAP.[38] The resulting pure monomers (Fig. 1) demonstrate a capability to dissolve some thermoplastics, such as PS and PMMA. 3D printing of 1,3-diether-2-methacrylate monomers containing varying fractions of dissolved PS and PMMA, in the presence of BAPO as a photoinitiator, resulted in the formation of polymer blends *via* a process distinct from conventional melt or solution blending, which typically requires heating and mechanical mixing in an extruder or solvent medium. This promising approach significantly influences both the mechanical properties and the microstructure of the resulting blend, which will be discussed in the following sections. In this study, wPS (M_w = 174.7 kDa), low molecular weight PS (M_w = 45 kDa), and PMMA (M_w = 15 kDa) were dissolved in the three different 1,3-diether-2-methacrylate monomers at 5 and 10 wt% to evaluate the influence of PS and PMMA on the properties of the resulting 3D printed polymer blends. The thermoplastic loadings were selected based on polymer solubility, resin viscosity, and SLA printability. Although MAA-DEP could dissolve up to 15 wt% wPS, formulations at this loading exhibited excessively high viscosity and could not be printed reliably, resulting in part adhesion to the resin tank even at extended exposure times. In contrast, PMMA loadings above 10 wt% were not fully soluble, leading to heterogeneous resins. Therefore, 5 and 10 wt% loadings were chosen as the highest compositions that ensured complete dissolution and reproducible printing while enabling evaluation of the effect of thermoplastic content on phase morphology and properties. The physical appearance of pure polymer and 3D-printed poly(1,3-diether-2-methacrylate)/PS or PMMA is shown in Fig. 2. The incorporation of PS notably altered the color and transparency of the resulting 3D-printed specimens, leading to yellowish blends. In contrast, PMMA-based blends retained some degree of transparency, particularly at lower concentrations, highlighting their better compatibility and optical clarity with the poly(MAA-DEP) matrix.

3.2. Hansen solubility parameters

To further assess the miscibility of glycerol-derived methacrylate monomers with PS and PMMA, Hansen Solubility Parameters (HSPs) and relative energy differences (RED) were calculated (Table 1 and Table S1). HSP provides a useful framework for understanding polymer solubility in terms of intermolecular interactions relevant to solvation; however, they are not a perfect model, with reported accuracies of only ~67% for "good" solvents and even lower for polar polymers.[48] PS and PMMA were used as reference polymers with δ_D (dispersion), δ_P (polar), and δ_H (H-bonding) values of 18.5, 4.5, 2.9, and 18.6, 10.5, 5.1 $(MPa)^{1/2}$, respectively, and R_0 (interaction radius) of 8 $(MPa)^{1/2}$ (Table S1). The calculated RED factors for the methacrylate monomers with PS were typically <1 (0.6–0.7), indicating favorable compatibility and consistent with the observed dissolution of PS in 1,3-diether-2-methacrylate monomers. In contrast, the RED values for the same monomers with PMMA were closer to unity (0.9–1.1), suggesting marginal miscibility. Interestingly, despite these predictions, PMMA is soluble in MAA-DEP, indicating that molecular weight, chain mobility, and processing conditions, factors not captured in HSP/RED calculations, can significantly influence experimental solubility.

3.3. Viscosity

Resin viscosity plays a crucial role in SLA 3D printing, significantly influencing print quality, mechanical properties, and the overall success of the printing process.[49] In general, relatively low viscosity is preferred to ensure proper recoating of the liquid resin between the previously cured layer and the resin tank surface.[50] Formulations with viscosities <5000 mPa s (5000 cP) are within the capabilities of SLA printers, ensuring proper layer recoating and adhesion during the printing process.[51] Table 2 summarizes the viscosities of the pure monomers and their corresponding PS and PMMA solutions at ~25 °C and atmospheric pressure. The pure 1,3-diether-2-methacrylate monomers exhibit low viscosities at 25 °C, ranging from 2.5 to 5.5 mPa s. The dissolution of PS and PMMA into the monomers significantly increases resin viscosity. For example, incorporating 5 and 10 wt% of wPS into MAA-DEP raises the viscosity to 44.1 and 166.2 mPa s, respectively. Higher monomer viscosity generally results in higher PS solution viscosity, with the MAA-DMEP/PS (10 wt%) solution exhibiting the highest value of 428.6 mPa s among the systems studied. In contrast, dissolving lower molecular weight PS, PS (45k), at 10 wt% in MAA-DEP resulted in a lower viscosity. The lowest viscosities among the polymer solutions, 5.2 and 10.7 mPa s, were observed for 5 and 10 wt% low molecular

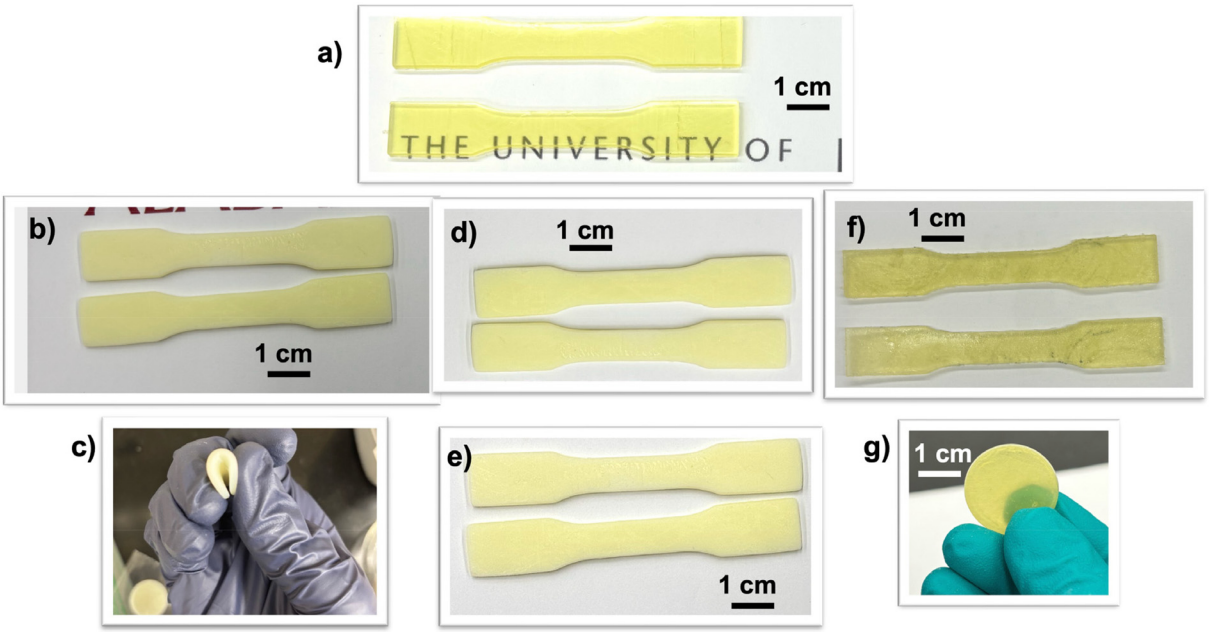

Fig. 2 Physical appearance of 3D-printed (a) neat poly(MAA-DEP) and 3D-printed poly(1,3-diether-2-methacrylate)/thermoplastic blends: (b) poly (MAA-DEP)/wPS (5 wt%), (c) poly(MAA-DEP)/wPS (10 wt%), (d) poly(MAA-DBP)/wPS (10 wt%), (e) poly(MAA-DMEP)/wPS (10 wt%) (f) poly(MAA-DEP)/PMMA (5 wt%), and (g) poly(MAA-DEP)/PMMA (10 wt%). Tensile bar specimens' dimensions (according to ASTM D 638 standards): 82 mm × 12 mm × 2 mm.

Table 1 Calculated HSP parameters of the 1,3-diether-2-methacrylates monomers and their R_a and (relative energy difference) RED values with the respective polymers

				R_a ((MPa)$^{1/2}$)		RED	
Monomers	δ_d ((MPa)$^{1/2}$)	δ_p ((MPa)$^{1/2}$)	δ_h ((MPa)$^{1/2}$)	PS	PMMA	PS	PMMA
MAA-DEP	16.0	4.7	5.0	5.4	7.8	0.7	1.0
MAA-DBP	16.1	3.7	4.2	5.0	8.5	0.6	1.1
MAA-DMEP	16.2	5.3	6.3	5.8	7.2	0.7	0.9

δ_D: dispersion forces. δ_P: polar interactions. δ_H: hydrogen-bonding interactions. RED = R_a/R_0.

Table 2 Viscosity (μ) of 1,3-diether-2-methacrylates monomers and their PS and PMMA solutions

Sample	μ (mPa s)
MAA-DEP	2.80
MAA-DEP/wPS (5 wt%)	44.1
MAA-DEP/wPS (10 wt%)	166.2
MAA-DEP/PS(45k) (10 wt%)	17.7
MAA-DEP/PMMA (5 wt%)	5.2
MAA-DEP/PMMA (10 wt%)	10.7
MAA-DBP	5.53
MAA-DBP/wPS (10 wt%)	284.1
MAA-DMEP	4.95
MAA-DMEP/wPS (10 wt%)	428.6

weight PMMA solutions in MAA-DEP. All formulations developed in this study demonstrated viscosities suitable for use in vat photopolymerization-based printing. However, since PS or PMMA lack reactive functional groups for photopolymerization, it is likely to interfere with the curing of active monomers, potentially influencing the final material properties.

3.4. Degree of conversion (DC, %)

The degree of C=C double bond conversion (DC%) in SLA 3D printing refers to the proportion of monomers that have polymerized into the solid structure during the curing process. A higher DC indicates a more complete polymerization, which significantly influences the mechanical properties and overall performance of the printed material. Fig. S1 presents the FTIR spectra of the 1,3-diether-2-methacrylate monomer blended with dissolved PS or PMMA, both before and after 3D printing. In most of the studied systems, the characteristic C=C stretching peak at 1638 cm^{-1} was almost eliminated after 3D printing, indicating efficient polymerization. However, in certain polymer blends—such as poly(MAA-DEP)/PS(45k) (10 wt%) and poly(MAA-DBP)/wPS (10 wt%)—this peak persisted with

Table 3 Degree of conversion (DC, %) of 3D-printed polymer blend

Printed blend	DC (%)
Poly(MAA-DEP)	78.3
Poly(MAA-DEP)/wPS (5 wt%)	84.7
Poly(MAA-DEP)/wPS (10 wt%)	80.6
Poly(MAA-DEP)/PS(45k) (10 wt%)	68.9
Poly(MAA-DBP)	82.1
Poly(MAA-DBP)/wPS (10 wt%)	44.8
Poly(MAA-DMEP)	80.7
Poly(MAA-DMEP)/wPS (10 wt%)	77.1
MAA-DEP/PMMA (5 wt%)	85.8
MAA-DEP/PMMA (10 wt%)	84.6

reduced intensity. Table 3 summarizes the DC calculated from eqn (1) for the 3D-printed 1,3-diether-2-methacrylate polymers containing 5 and 10 wt% of PS and PMMA. Blending poly (MMA-DEP) with wPS preserved high polymerization efficiency, achieving DC values >80%. This suggests that the increased viscosity of the 10 wt% wPS solution did not hinder C═C double bond conversion. The incorporation of 10 wt% PS (45 kDa) into MAA-DEP reduced the DC to 68.9%. This reduction is likely due to the PS chains interfering with the formation of a continuous polymer matrix, possibly through the formation of microdomains that disrupt network uniformity. A notably lower DC (44.8%) was observed for the poly (MAA-DBP)/wPS (10 wt%) blend. The significant reduction may stem from the greater interference of wPS with the curing of MAA-DBP, whose longer alkyl side chains (compared to MAA-DEP) introduce additional steric hindrance and reduce compatibility during network formation. As will be shown later, the SEM images clearly illustrate the resulting differences in phase structure. However, the poly(MAA-DMEP)/wPS (10 wt%) blend exhibited a relatively high DC of 77.1%, despite having the highest viscosity among the systems studied. This suggests that the more flexible chemical structure of the DMEP monomer may facilitate better compatibility or interaction with wPS, enabling more efficient polymerization under high-viscosity conditions. These findings highlight the significant impact of PS molecular weight and chemical structure of the monomer on the polymerization efficiency of SLA-printed blends.

Dissolving PMMA into MAA-DEP at both 5 and 10 wt% resulted in high DC values of 85.8% and 84.6%, respectively. Unlike the PS blends, the PMMA blends remained optically transparent (Fig. 2f and g) to some extent and highly flexible, likely due to excellent molecular-level dispersion of PMMA within the matrix. The structural similarity between PMMA and the poly(methacrylate) matrix likely enhances miscibility and interfacial compatibility, reducing phase separation and optical scattering that could otherwise impede light penetration and hinder efficient photopolymerization.

3.5. Mechanical properties

The mechanical performance of the 3D-printed polymer blends was evaluated *via* tensile testing, with results reported in terms of tensile strength, Young's modulus, and elongation at break (Fig. 3 and Table S2). The mechanical behavior of the pristine 3D-printed monomers has been previously reported; among them, poly(MAA-DEP) exhibited the best performance, displaying a characteristic elastic response with a tensile strength of 1.61 MPa, Young's modulus of 7.67 MPa, and elongation at break of 142.94%.[38]

The incorporation of PS into 1,3-diether-2-methacrylate polymers generally enhanced the tensile strength and stiffness of the resulting blends while reducing their elongation at break. This trend is attributed to the reinforcing effect of PS, which inherently possesses high tensile strength and rigidity, but also introduces brittleness into the system. For example, blending 5 wt% wPS with poly(MAA-DEP) significantly increased the tensile strength (3.5 MPa) and modulus (22.6 MPa) compared to the neat resin; however, the elongation at break dropped sharply to 24.2% (Fig. 3). Interestingly, increasing the wPS loading to 10 wt% in poly(MAA-DEP) further enhanced strength and stiffness, while the elongation at break recovered to ~90%. This behavior suggests that the dispersion of the PS domain and phase morphology in the resulting blend are influenced by composition, as will be further examined in the following microstructure analysis section. The incorporation of 10 wt% PS(45k) into poly(MAA-DEP) yielded lower tensile strength (2.2 MPa) and modulus (12.6 MPa), along with limited elongation (~29%) (Fig. 3d and Table S2). The inferior performance is likely due to lower molecular weight, reduced chain entanglement, and weaker phase interaction between the short-chain PS and the matrix. The poly(MAA-DBP)/wPS (10 wt%) formulation exhibited a relatively high tensile strength of 3.9 MPa and the highest Young's modulus of 30.7 MPa, primarily due to the intrinsically rigid nature of the poly(MAA-DBP) matrix and the reinforcing effect of the incorporated PS. However, the elongation at break decreased to ~20%, indicating limited elasticity (Fig. 4d). The poly(MAA-DMEP)/wPS (10 wt%) blend exhibited significantly enhanced mechanical strength and stiffness, over threefold and ninefold increases, respectively, compared to its neat counterpart, likely due to improved interfacial interaction between the two polymers. However, its elongation at break was reduced to ~27%.

The incorporation of PMMA into poly(MAA-DEP) led to noticeable changes in mechanical performance. At 5 wt%, PMMA improved the elongation at break to 159.2%, surpassing even the pristine polymer and all PS-containing blends. This remarkable elasticity is likely due to better dispersion of PMMA domains and favorable interaction between low molecular weight PMMA and the poly(MAA-DEP) matrix, enabling more energy dissipation during deformation. While the tensile strength remained comparable to the neat polymer (1.80 MPa *vs.* 1.6 MPa for pure polymer), the Young's modulus decreased slightly to 6.6 MPa at low PMMA loading. At 10 wt%, the increased content of PMMA led to significant improvements in tensile strength (3.1 MPa) and Young's modulus (10.0 MPa) without a significant change in elongation at break. This behavior contrasts with the trends observed in PS blends, which exhibited low elongation at break, underscoring the favorable nature of PMMA-matrix interactions despite its low molecular weight.

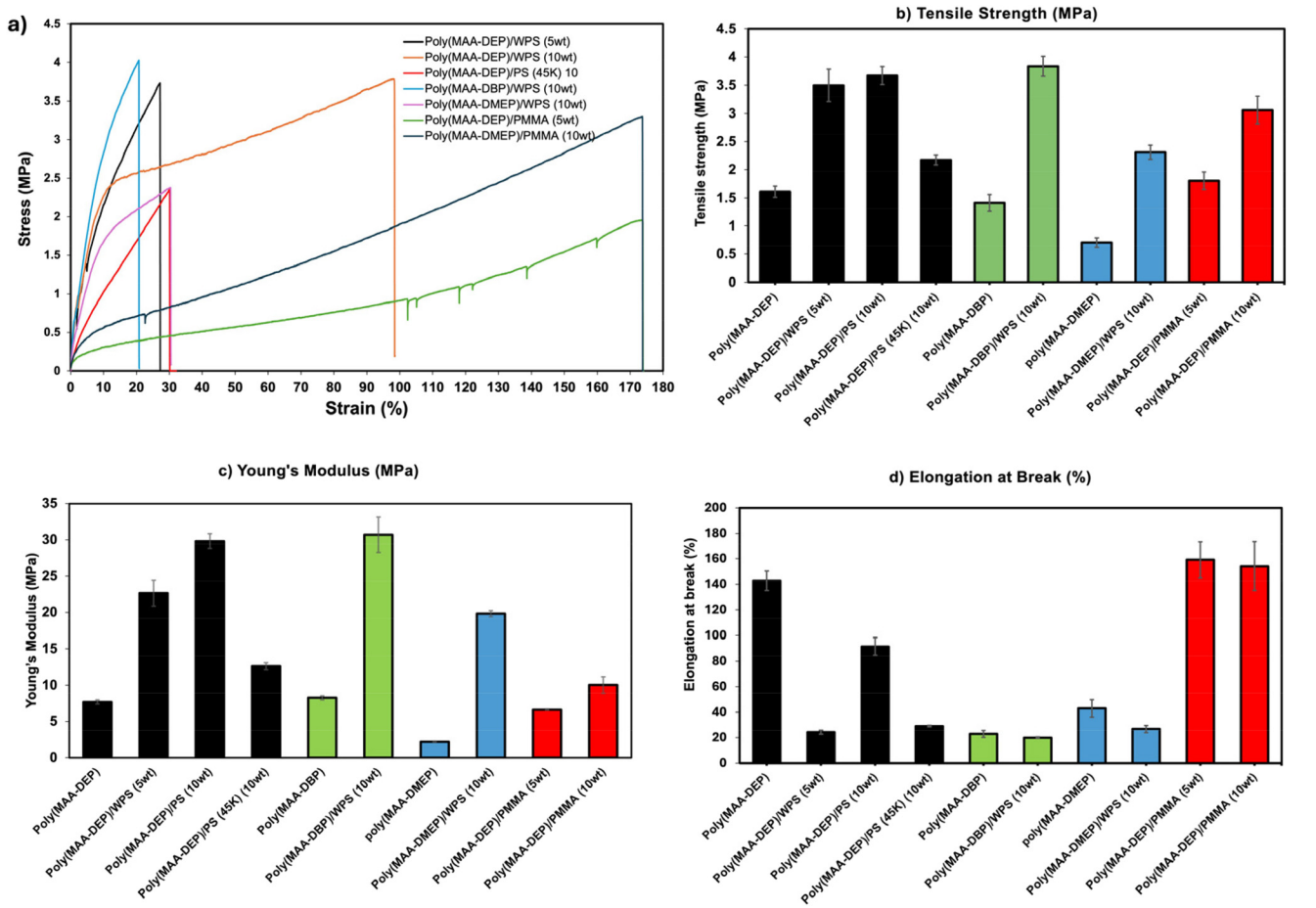

Fig. 3 Mechanical properties of 3D-printed poly(1,3-diether-2-methacrylate)/thermoplastic blends. (a) Stress–strain curves (the curves correspond to representative individual tensile tests near the mean mechanical response), (b) tensile strength, (c) Young's modulus, and (d) elongation at break (%) for various 3D-printed blends incorporating 5 and 10 wt% PS or PMMA. Bars represent the mean values for each formulation. Error bars represent the standard error of the mean (SEM).

3.6. Thermal properties

3.6.1. DSC. DSC was conducted to investigate the T_gs of the SLA 3D-printed polymer blends. The resulting thermograms are presented in Fig. S2–S9, and the corresponding T_g values are summarized in Table 4. Three heating–cooling cycles were performed to ensure reliable results; the first cycle (green curve in the DSC thermograms) was discarded to eliminate thermal history, and the T_g was determined from the average of the second and third cycles.

DSC thermograms of pure 1,3-diether-2-methacrylate polymers, wPS, PS (45k) and PMMA are shown in Fig. S2. Among the pure polymers, poly(MAA-DEP) exhibited the lowest T_g, measured at 0.29 °C. The glass transition behavior of a polymer blend is a key indicator of its phase miscibility. While fully miscible blends exhibit a single T_g somewhere between the T_gs of the two pure components, immiscible blends typically exhibit two distinct T_g values corresponding to those of the pure components, indicating the presence of two separate phases.[52] DSC analysis of the 3D-printed PS blends revealed two distinct T_gs in all samples: one corresponding to the main matrix, 1,3-diether-2-methacrylate polymers (T_{g1}), and the other to the PS or PMMA phase (T_{g2}), indicating that the two polymers are immiscible. However, the T_g peaks of the resulting polymer blends are generally broadened and slightly shifted compared to those of the corresponding pure polymers. For instance, the T_g of poly(MAA-DEP) containing 10 wt% wPS increased slightly to 0.72 °C with a broadened peak. In contrast, the blend containing 5 wt% wPS exhibited a decreased T_g of −2.28 °C, suggesting composition-dependent variations in segmental mobility and possible phase interactions between PS and the poly(MAA-DEP) matrix. Such T_g shifts and broadening are commonly attributed to partial miscibility between the polymer phases, particularly at interfacial regions.[53,54] The T_g associated with the PS phase was consistently reduced across all blends. Residual unreacted monomers likely act as plasticizers, diffusing into the PS domains and reducing their T_g through enhanced segmental mobility and interfacial molecular interpenetration.

The poly(MAA-DEP)/PMMA blends also exhibited two T_g values. For the 5 wt% PMMA blend, the T_g of the matrix (T_{g1}) and the PMMA phase (T_{g2}) decreased to −6.39 °C and

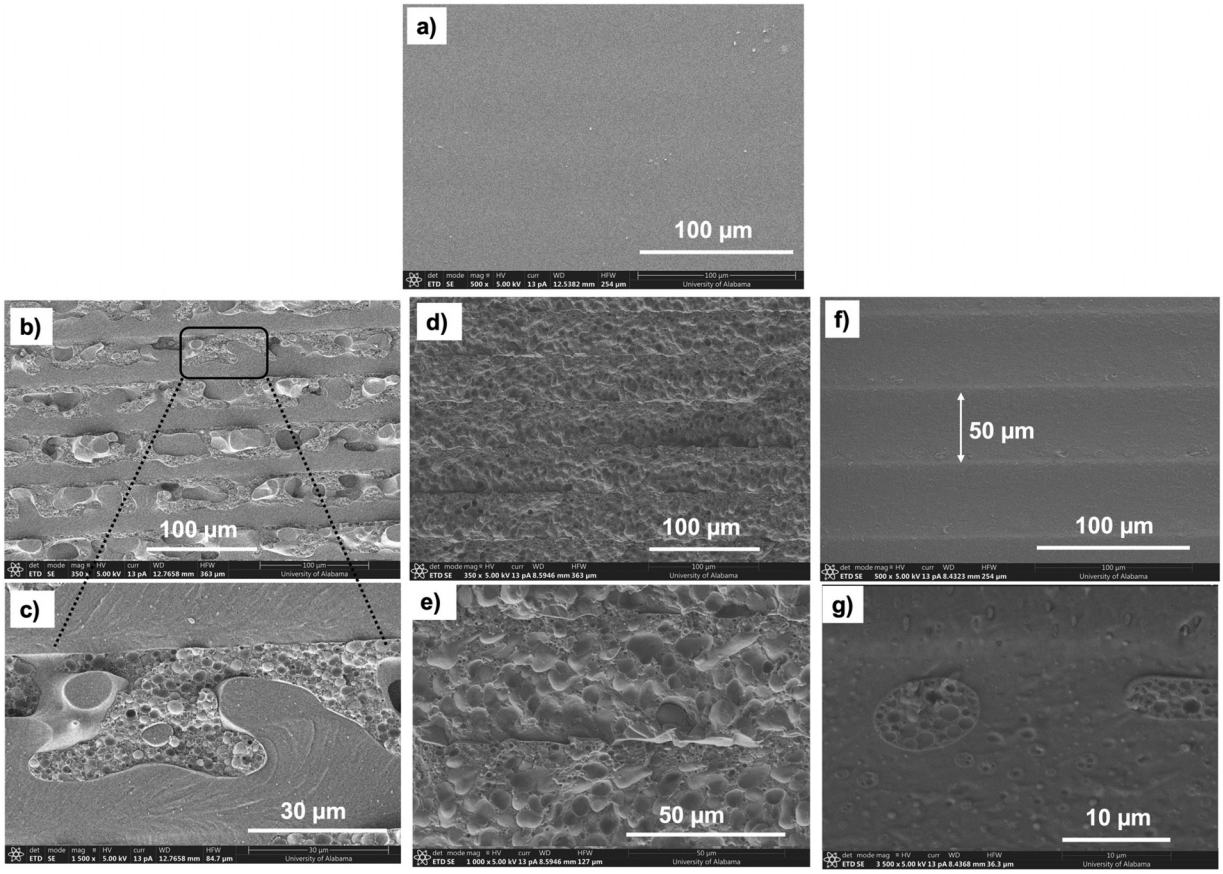

Fig. 4 SEM images of cryofracture surface of 3D printed (a) pure poly(MAA-DEP), b and (c) poly(MAA-DEP)/wPS (5 wt%), d and (e) poly(MAA-DEP)/wPS (10 wt%) and f and (g) poly(MAA-DEP)/PS(45k) (10 wt%).

Table 4 Thermal properties of 1,3-diether-2-methacrylate polymers and their blends with PS and PMMA

Sample	T_{g1} [a] (°C)	T_{g2} [b] (°C)	$T_{d,max1}$ [c] (°C)	$T_{d,max2}$ [d] (°C)
Poly(MAA-DEP)	0.29	—	291	—
wPS	—	103.73	—	410
Poly(MAA-DEP)/wPS (5 wt%)	−2.28	80.6	331	431
Poly(MAA-DEP)/wPS (10 wt%)	0.72	95.82	309	395
PS (45k)	—	60.72	—	405
Poly(MAA-DEP)/PS45 (10 wt%)	−0.92	59.04	338	416
Poly(MAA-DBP)	27.17	—	326	—
Poly(MAA-DBP)/wPS (10 wt%)	27.11	89.49	301	419
Poly(MAA-DMEP)	26.17	—	309	—
Poly(MAA-DMEP)/wPS (10 wt%)	22.77	71.88	351	420
PMMA	—	80.50	—	361
Poly(MAA-DEP)/PMMA (5 wt%)	−6.39	77.11	326	—
Poly(MAA-DEP)/PMMA (10 wt%)	−0.80	74.31	324	410

[a] T_g of main polymer matrix. [b] T_g of PS or PMMA phase. [c] Primary maximum decomposition temperature of polymer matrix as measured by TGA. [d] Secondary maximum decomposition temperature of PS or PMMA component.

77.11 °C, respectively. The reduction in T_{g1} at low PMMA content implies enhanced segmental mobility in the matrix, likely due to the good dispersion of low molecular weight PMMA and partial intermixing at the molecular level, which increases free volume and reduces T_g. The structural similarity between the two polymers may promote this compatibility, facilitating better dispersion and interfacial adhesion. At a higher PMMA content (10 wt%), the diminished T_{g1} depression suggests more significant phase separation, reducing the extent of interfacial mixing and its influence on matrix mobility. The decrease in T_{g2} associated with the PMMA phase was also observed for these blends, attributed to

enhanced chain mobility, likely due to interfacial mixing with the surrounding matrix and the presence of unreacted monomers. This interaction may locally disrupt PMMA's chain packing and reduce its T_g.

The more pronounced T_{g2} shifts observed for the wPS-containing blends might be attributed to the polydisperse nature of the waste polystyrene. Although the M_w of wPS is relatively high (174.7 kDa), its broad molecular weight distribution (PDI = 2.31)[45] implies the presence of a significant fraction of lower-molecular-weight chains. These shorter PS chains are likely to be more susceptible to partial interpenetration into the poly (methacrylate) matrix and to plasticization by residual monomers, leading to greater T_g depression.

3.6.2. TGA. TGA and DTG thermograms of the 1,3-diether-2-methacrylate polymer blends containing PS and PMMA are presented in Fig. S10, and the $T_{d,max}$ values for the primary and secondary degradation steps are summarized in Table 4. As shown, the thermal stability of almost all blends improved relative to the neat polymers of the 1,3-diether-2-methacrylates reported previously.[38] Nearly all PS blends exhibited a dominant degradation step between 300 °C and 350 °C, corresponding to the decomposition of the 1,3-diether-2-methacrylate matrix, followed by a secondary, minor degradation step attributed to the PS phase. Fig. S10b, d, and f show the DTG curves of the blends and pure PS and PMMA, which depict the corresponding degradation steps. The primary maximum decomposition temperature of the main polymer matrix ($T_{d,max1}$) increased modestly in most blends compared to neat polymers (Table 4), indicating enhanced thermal stability upon blending. For instance, $T_{d,max1}$ for Poly(MAA-DEP) increased from 291 °C (pure polymer) to 331 °C and 309 °C upon incorporating 5 and 10 wt% wPS, respectively. However, not all blends resulted in stabilization. An exception was observed for the poly(MAA-DBP)/wPS (10 wt%) blend, which exhibited a slight decrease in $T_{d,max1}$ from 326 °C (neat polymer) to 301 °C. This reduction supports the hypothesis of incomplete polymer formation in the presence of wPS, consistent with the lower DC reported for this system. Interestingly, while the $T_{d,max2}$ values for the PS components remained close to their respective pure polymer degradation temperatures (410 °C) in most blends, a notable decrease to 395 °C was observed for the poly(MAA-DEP)/wPS (10 wt%) system. This reduction may be attributed to improved dispersion of PS and increased interfacial interactions or chain entanglement with the less thermally stable matrix, which could promote the earlier onset of wPS degradation. However, interpreting these changes remains complex, as the thermal behavior of polymer blends often deviates from that of the individual components.[55] Literature reports varying outcomes during the co-pyrolysis of mixed thermoplastics, with both synergistic stabilization and accelerated degradation observed depending on interactions between different species in the blend and their respective degradation products.[56,57] In contrast to the wPS-containing blends, increasing the PMMA content from 5 to 10 wt% in the poly(MAA-DEP) matrix did not significantly change the thermal stability, with $T_{d,max1}$ increasing to ~325 °C for both. The second degradation step was not clearly resolved in the 5 wt% PMMA blend. Since PMMA has a lower degradation temperature than PS, its degradation might overlap more closely with that of the main polymer matrix (poly(MAA-DEP)).

3.7. Morphology analysis by SEM

Microstructural analysis of the 3D-printed polymer blends was conducted using SEM to investigate phase morphology and domain dispersion (Fig. 4 and 5, and S11). Most polymer blends are thermodynamically immiscible because the mixing of high-molecular-weight chains results in minimal entropy gain. In contrast, the enthalpy of mixing is typically positive, making the overall process energetically unfavorable. Additionally, the high viscosities of the individual polymers hinder phase mobility and coalescence, resulting in kinetically trapped, partially mixed systems. Consequently, conventional blending techniques such as extrusion or internal mixing often yield phase-separated morphologies, with domain sizes typically ranging from 0.1 to 50 μm. PS, a non-polar polymer with a rigid backbone, tends to be immiscible with many polar or flexible polymers due to unfavorable enthalpic interactions, often leading to phase separation in the resulting blends.[58] The remarkable ability of the synthesized 1,3-diether-2-methacrylates in dissolving PS with different molecular weights and their application in SLA 3D printing leads to polymer blends with interesting and distinct morphology depending on the PS content and molecular weight. The cryofracture surface of 3D-printed poly(MAA-DEP) (Fig. 4a) displayed a smooth, homogeneous morphology without visible layer lines, suggesting uniform curing and strong interlayer adhesion. Fig. 4b and c show the fracture surface of the 3D-printed blend containing 5 wt% wPS in MAA-DEP with different magnifications. Unlike the smooth morphology observed in the pure poly(MAA-DEP), these images reveal layer-by-layer curing patterns characteristic of the SLA 3D printing process. At low PS concentrations, SEM analysis reveals that during 3D printing, the dissolved PS tends to migrate toward the top of each printed layer, forming PS-rich regions that are phase-separated from the main poly (MAA-DEP) matrix. The PS-rich regions themselves are characterized by spherical PS domains dispersed within the remaining poly(MAA-DEP) matrix. This creates a stratified microstructure, with each layer exhibiting a distinct boundary between the flexible matrix and the rigid PS domains. Such morphology disrupts the uniform stress distribution during deformation and introduces stress concentration points at the matrix–domain interfaces, resulting in a substantial loss of elasticity (Fig. 3d).

SEM analysis of the 3D-printed poly(MAA-DEP) blend containing 10 wt% wPS (Fig. 4d and e) reveals a markedly different microstructure compared to the 5 wt% sample. At the higher loading, PS appears more uniformly dispersed as discrete domains within the polymer matrix, suggesting improved trapping during photopolymerization. This behavior might be attributed in part to the higher resin viscosity at increased wPS content, which restricts polymer chain mobility and sup-

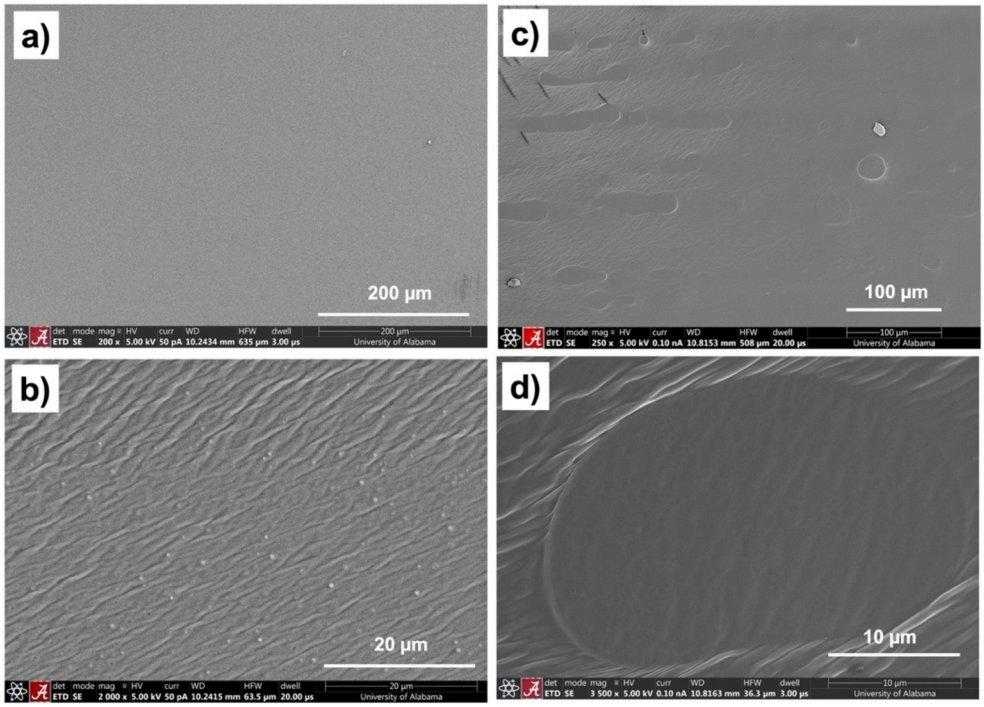

Fig. 5 SEM images of cryofractured surface of (a) and (b) poly(MAA-DEP)/PMMA (5 wt%), c and (d) poly(MAA-DEP)/PMMA (10 wt%).

presses long-range phase migration during the layer-by-layer curing process. Although some heterogeneity persists, evident from the slightly higher PS domain concentration with smaller size near the top of each printed layer, the overall morphology shows the wPS phase is well dispersed compared to the blend with 5 wt%. By limiting PS mobility prior to gelation, the increased viscosity promotes kinetic stabilization of the dispersed phase, resulting in reduced stratification. This improved dispersion of PS domains contributes directly to the enhanced mechanical performance of the blend, leading to a significant recovery in elongation at break. These observations highlight resin viscosity as a key formulation parameter governing microstructure development and mechanical performance in SLA-printed polymer blends. However, SEM analysis of the poly(MAA-DEP) blend containing 10 wt% low molecular weight PS, PS(45k), reveals that spherical PS domains with different sizes from <1 μm to >10 μm are dispersed within the continuous poly(MAA-DEP) matrix. Additionally, larger PS domains consisting of aggregated smaller ones suggest incomplete coalescence or secondary phase separation during printing and curing. This morphology contrasts with the more uniformly dispersed structure observed for blends containing higher-molecular-weight PS.

The 3D-printed poly(MAA-DBP)/wPS (10 wt%) blend exhibited a distinctly different morphology, resembling a honeycomb-like droplet structure (Fig. S11a and b), which highlights the sensitivity of microstructure development to slight variations in monomer chemical structure. The larger droplets of the main matrix are observed at the bottom of each printed layer, encapsulated or surrounded by small PS domains (~1 μm), while smaller matrix droplets dominate the top. This gradient structure indicates upward migration of the PS phase during curing, with the domains exhibiting relatively well-defined boundaries, indicative of poor miscibility and limited interfacial mixing between PS and the main matrix. The cryofractured surfaces of 3D-printed poly(MAA-DMEP) containing 10 wt% wPS exhibit a uniform dispersion of PS domains throughout the matrix (Fig. S11c and d). However, the layer boundaries appear more distinct compared to other systems, indicating less effective interlayer fusion during the SLA printing process.

SEM images of 3D-printed poly(MAA-DEP) blends containing 5 wt% and 10 wt% PMMA are presented in Fig. 5. At a lower magnification, Fig. 5a, the 5 wt% PMMA blend exhibits a homogeneous appearance, without characteristic layer-by-layer deposition patterns typically observed in 3D-printed PS-based blends. However, higher magnification (Fig. 5b) reveals a dilute droplet-matrix morphology, characterized by spherical PMMA domains approximately 1 μm in diameter dispersed within the continuous poly(MAA-DEP) matrix. Such morphology is common in blends with low concentrations of the dispersed phase.[59] The interfacial adhesion between PMMA droplets and the poly(MAA-DEP) matrix, arising from favorable interactions between their ester functionalities, can enhance interfacial compatibility and reduce phase separation. These interactions facilitate more uniform stress distribution during deformation, promoting energy dissipation and contributing to improved elasticity and toughness[60] (Fig. 3d). In contrast, the 10 wt% PMMA blend (Fig. 5c) exhibits larger, oval-shaped PMMA domains with less uniform dispersion, predominantly

concentrated near the top of each printed layer with no distinct interlayer boundaries. Despite the significantly increased domain size, these PMMA regions maintain strong interfacial adhesion with the poly(MAA-DEP) matrix, as evidenced in Fig. 5d. The presence of larger domains may introduce stress concentration points; however, the overall matrix continuity is preserved, with the polymer matrix connected at several locations across each layer. This interconnected structure contributes to a continuous matrix, which is essential for maintaining mechanical integrity.

4. Conclusions

In this study, glycerol-derived 1,3-diether-2-methacrylate monomers were synthesized and employed as dual-function molecules, serving as both photopolymerizable monomers and solvents to dissolve thermoplastics such as PS and PMMA. These formulations were used to fabricate polymer blends *via* SLA 3D printing to investigate the effects of thermoplastic incorporation on morphology, mechanical, and thermal properties. The blends exhibited distinct phase separation depending on monomer structure, thermoplastic structure, and loading. All polymer blends displayed two T_g values, indicating the formation of immiscible systems; however, peak broadening and slight shifts suggest partial miscibility at the interface. The poly(MAA-DEP)/wPS system with low concentrations of wPS led to pronounced phase separation and a loss of elasticity, while increasing the wPS content to 10 wt% improved PS domain dispersion, enabling recovery of elongation at break, and more favorable mechanical properties. Incorporation of low-molecular-weight PMMA, with a structure closer to that of glycerol-derived 1,3-diether-2-methacrylate polymers, particularly at lower concentrations, yields a continuous polymer matrix with indistinguishable printed layer boundaries and a slight increase in elongation at break.

This method provides an alternative to conventional blend formation, which typically relies on melt-blending polymers in an extruder. In contrast, the approach demonstrated here enables blend formation through photopolymerization in the presence of dissolved thermoplastics, thereby reducing energy input and processing complexity. Importantly, the potential use of waste PS and PMMA in these systems offers a promising route to reuse two of the most widely produced thermoplastics, aligning with circular economy principles. Further optimization through a more sophisticated monomer design with different types of functional groups (*e.g.*, aromatics) and/or non-symmetric functional groups (*e.g.*, one alkyl chain, one aromatic group) and/or through the inclusion of crosslinkers or compatibilizers could enhance material performance and expand the range of potential applications and types of polymers that could be dissolved. Nonetheless, it is clear that the use of glycerol-derived 1,3-diether-2-methacrylates offer a very wide range of design possibilities for sustainable and advanced SLA 3D printing resin formulations.

Conflicts of interest

There are no conflicts to declare.

Data availability

The data supporting this article have been included as part of the supplementary information (SI). Supplementary information: detailed synthesis of symmetric 1,3-diether-2-methacrylates. Scheme S1. General synthesis of 1,3-diether-2-methacrylates. Table S1. Hansen solubility parameters (HSP) of PS and PMMA polymers. Table S2. Tensile properties of the 3D printed pure polymers and their blends. Fig. S1. FTIR spectra of poly(1,3-diether-2-methacrylate)/thermoplastic blends. Fig. S2. DSC thermograms of pure polymers. Fig. S3. DSC thermograms of poly(MAA-DEP)/WPS (5 wt%). Fig. S4. DSC thermograms of poly(MAA-DEP)/WPS (10 wt%). Fig. S5. DSC thermograms of poly(MAA-DEP)/PS(45k) (10 wt%). Fig. S6. DSC thermograms of poly(MAA-DBP)/WPS (10 wt%). Fig. S7. DSC thermograms of poly(MAA-DMEP)/WPS (10 wt%). Fig. S8. DSC thermograms of poly(MAA-DEP)/PMMA (5 wt%). Fig. S9. DSC thermograms of poly(MAA-DEP)/PMMA (10 wt%). Fig. S10. TGA and DTG thermograms of poly(1,3-diether-2-methacrylate)/thermoplastic blends. Fig. S11. SEM images of cryofracture surface of a and (b) poly(MAA-DBP)/WPS (10 wt%), c and (d) poly(MAA-DMEP)/WPS (10 wt%). See DOI: https://doi.org/10.1039/d6lp00005c.

Acknowledgements

Support for this work provided by the US National Science Foundation (EFMA-2029387) is gratefully acknowledged. During the preparation of this work the author(s) used Adobe Firefly to generate portions of the TOC graphic. After using this tool/service, the authors reviewed and edited the content as needed and take full responsibility for the content of the published article. The authors' university has a license for Adobe Firefly and terms of use associated with the software are being followed. All other images/photographs were fully created by the authors.

References

1 H. I. Mahdi, N. N. Ramlee, J. L. da Silva Duarte, Y.-S. Cheng, R. Selvasembian, F. Amir, L. H. de Oliveira, N. I. W. Azelee, L. Meili and G. Rangasamy, A comprehensive review on nanocatalysts and nanobiocatalysts for biodiesel production in Indonesia, Malaysia, Brazil and USA, *Chemosphere*, 2023, **319**, 138003.

2 S. Qian, X. Liu, G. P. Dennis, C. H. Turner and J. E. Bara, Properties of symmetric 1, 3-diethers based on glycerol skeletons for CO2 absorption, *Fluid Phase Equilib.*, 2020, **521**, 112718.

3 A. Zanoni, G. Gardoni, M. Sponchioni and D. Moscatelli, Valorisation of glycerol and CO_2 to produce biodegradable polymer nanoparticles with a high percentage of bio-based components, *J. CO_2 Util.*, 2020, **40**, 101192.
4 G. Dodekatos, S. Schünemann and H. Tüysüz, Recent advances in thermo-, photo-, and electrocatalytic glycerol oxidation, *ACS Catal.*, 2018, **8**(7), 6301–6333.
5 S. Basu and A. K. Sen, A review on catalytic dehydration of glycerol to acetol, *ChemBioEng Rev.*, 2021, **8**(6), 633–653.
6 D. Spataru, A. P. S. Dias and L. F. V. Ferreira, Acetylation of biodiesel glycerin using glycerin and glucose derived catalysts, *J. Cleaner Prod.*, 2021, **297**, 126686.
7 S. Qian, X. Liu, V. N. Emel'yanenko, P. Sikorski, I. Kammakakam, B. S. Flowers, T. A. Jones, C. H. Turner, S. P. Verevkin and J. E. Bara, Synthesis and properties of 1, 2, 3-Triethoxypropane: a glycerol-derived green solvent candidate, *Ind. Eng. Chem. Res.*, 2020, **59**(45), 20190–20200.
8 I. V. Andreeva, D. H. Zaitsau, S. Qian, V. V. Turovtzev, A. A. Pimerzin, J. E. Bara and S. P. Verevkin, Glycerol valorisation towards biofuel additivities: Thermodynamic studies of glycerol ethers, *Chem. Eng. Sci.*, 2022, **247**, 117032.
9 K. Pandit, C. Jeffrey, J. Keogh, M. S. Tiwari, N. Artioli and H. G. Manyar, Techno-economic assessment and sensitivity analysis of glycerol valorization to biofuel additives via esterification, *Ind. Eng. Chem. Res.*, 2023, **62**(23), 9201–9210.
10 L. D. da Silva, R. C. Santos, J. G. A. B. Silva, E. de Paiva Alves, R. T. F. Fréty and L. A. M. Pontes, Direct ammoxidation of glycerol to nitriles using Mo/alumina catalysts, *React. Kinet., Mech. Catal.*, 2022, 1–15.
11 N. Ebadipour, S. Paul, B. Katryniok and F. Dumeignil, Alkaline-based catalysts for glycerol polymerization reaction: A review, *Catalysts*, 2020, **10**(9), 1021.
12 M. Ionescu and Z. S. Petrović, On the Mechanism of Base–Catalyzed Glycerol Polymerization and Copolymerization, *Eur. J. Lipid Sci. Technol.*, 2018, **120**(6), 1800004.
13 F. Zeng, X. Yang, D. Li, L. Dai, X. Zhang, Y. Lv and Z. Wei, Functionalized polyesters derived from glycerol: Selective polycondensation methods toward glycerol–based polyesters by different catalysts, *J. Appl. Polym. Sci.*, 2020, **137**(16), 48574.
14 T. Ghosh and N. Karak, Biobased multifunctional macroglycol containing smart thermoplastic hyperbranched polyurethane elastomer with intrinsic self-healing attribute, *ACS Sustainable Chem. Eng.*, 2018, **6**(3), 4370–4381.
15 M. Forrester, A. Becker, A. Hohmann, N. Hernandez, F.-Y. Lin, N. Bloome, G. Johnson, H. Dietrich, J. Marcinko and R. C. Williams, RAFT thermoplastics from glycerol: a biopolymer for development of sustainable wood adhesives, *Green Chem.*, 2020, **22**(18), 6148–6156.
16 P. D. Pham, S. Monge, V. Lapinte, Y. Raoul and J. J. Robin, Various radical polymerizations of glycerol–based monomers, *Eur. J. Lipid Sci. Technol.*, 2013, **115**(1), 28–40.
17 A. Mhanna, F. Sadaka, G. Boni, C.-H. Brachais, L. Brachais, J.-P. Couvercelle, L. Plasseraud and L. Lecamp, Photopolymerizable synthons from glycerol derivatives, *J. Am. Oil Chem. Soc.*, 2014, **91**, 337–348.
18 X. Sun, J.-P. Lindner, B. Bruchmann and A. D. Schlüter, Synthesis of Neutral, Water-Soluble Oligo–Ethylene Glycol-Containing Dendronized Homo-and Copolymers of Generations 1, 1.5, 2, and 3, *Macromolecules*, 2014, **47**(21), 7337–7346.
19 F.-Y. Lin, B. Claypool, M. J. Forrester, N. Hernández, A. Buss, B. Kuehl and E. W. Cochran, Glycerol-Based Pressure Sensitive Adhesives: Synthesis and Applications, *ACS Sustainable Chem. Eng.*, 2024, **12**(32), 12042–12051.
20 L. Pichavant, C. Guillermain and X. Coqueret, Reactivity of vinyl ethers and vinyl ribosides in UV-initiated free radical copolymerization with acceptor monomers, *Biomacromolecules*, 2010, **11**(9), 2415–2421.
21 S. Goyal, F.-Y. Lin, M. Forrester, W. Henrichsen, G. Murphy, L. Shen, T.-P. Wang and E. W. Cochran, Glycerol ketals as building blocks for a new class of biobased (meth) acrylate polymers, *ACS Sustainable Chem. Eng.*, 2021, **9**(31), 10620–10629.
22 S. C. Ligon, R. Liska, J. Stampfl, M. Gurr and R. Mülhaupt, Polymers for 3D printing and customized additive manufacturing, *Chem. Rev.*, 2017, **117**(15), 10212–10290.
23 V. S. Voet, J. Guit and K. Loos, Sustainable photopolymers in 3D printing: a review on biobased, biodegradable, and recyclable alternatives, *Macromol. Rapid Commun.*, 2021, **42**(3), 2000475.
24 V. S. Voet, Closed-loop additive manufacturing: dynamic covalent networks in vat photopolymerization, *ACS Mater. Au*, 2022, **3**(1), 18–23.
25 E. M. Maines, M. K. Porwal, C. J. Ellison and T. M. Reineke, Sustainable advances in SLA/DLP 3D printing materials and processes, *Green Chem.*, 2021, **23**(18), 6863–6897.
26 E. Skliutas, M. Lebedevaite, S. Kasetaite, S. Rekštytė, S. Lileikis, J. Ostrauskaite and M. Malinauskas, A bio-based resin for a multi-scale optical 3D printing, *Sci. Rep.*, 2020, **10**(1), 9758.
27 J. Stouten, G. H. Schnelting, J. Hul, N. Sijstermans, K. Janssen, T. Darikwa, C. Ye, K. Loos, V. S. Voet and K. V. Bernaerts, Biobased photopolymer Resin for 3D printing containing dynamic imine bonds for fast reprocessability, *ACS Appl. Mater. Interfaces*, 2023, **15**(22), 27110–27119.
28 L. Pezzana, R. Wolff, J. Stampfl, R. Liska and M. Sangermano, High temperature vat photopolymerization 3D printing of fully bio-based composites: Green vegetable oil epoxy matrix & bio-derived filler powder, *Addit. Manuf.*, 2024, **79**, 103929.
29 J. Guit, M. B. Tavares, J. Hul, C. Ye, K. Loos, J. Jager, R. Folkersma and V. S. Voet, Photopolymer resins with biobased methacrylates based on soybean oil for stereolithography, *ACS Appl. Polym. Mater.*, 2020, **2**(2), 949–957.
30 S. Miao, W. Zhu, N. J. Castro, M. Nowicki, X. Zhou, H. Cui, J. P. Fisher and L. G. Zhang, 4D printing smart biomedical scaffolds with novel soybean oil epoxidized acrylate, *Sci. Rep.*, 2016, **6**(1), 27226.

31 K. P. Cortés-Guzmán, A. R. Parikh, M. L. Sparacin, A. K. Remy, L. Adegoke, C. Chitrakar, M. Ecker, W. E. Voit and R. A. Smaldone, Recyclable, biobased photoresins for 3d printing through dynamic imine exchange, *ACS Sustainable Chem. Eng.*, 2022, **10**(39), 13091–13099.
32 S. Chatterjee, S. Qian, A. Soyemi, T. Szilvási and J. E. Bara, Synthesis and Properties of 2-Halo-1, 3-diether-propanes: Diversifying the Range of Functionality in Glycerol-Derived Compounds, *Ind. Eng. Chem. Res.*, 2023, **62**(6), 2959–2967.
33 S. Qian, X. Liu, C. H. Turner and J. E. Bara, Synthesis and properties of symmetric glycerol-derived 1, 2, 3-triethers and 1, 3-diether-2-ketones for CO2 absorption, *Chem. Eng. Sci.*, 2022, **248**, 117150.
34 S. Qian, J. D. Leah, S. Chatterjee, A. Soyemi, T. Szilvási and J. E. Bara, Properties of Imidazolium Ionic Liquids with Glycerol-Derived Functional Groups, *J. Chem. Eng. Data*, 2022, **67**(8), 1905–1914.
35 J. Wang, S. Qian, G. Olajide, S. Chatterjee, T. Szilvasi and J. E. Bara, Synthesis and properties of symmetric glycerol-derived (E/Z)-1, 3-diether-2-alkenes, *Ind. Chem. Mater.*, 2026, **4**, 131–141.
36 G. Lingua, G. Depraetère, J. Wang, J. E. Bara, M. Forsyth and D. Mecerreyes, Solvate Ionic Liquids based on branched glymes enabling high performance lithium metal batteries, *J. Power Sources*, 2024, **624**, 235535.
37 J. Wang, M. Iddrisu, Z. S. Pour, S. Ravula, T. Szilvási and J. E. Bara, Synthesis and Properties of Novel Glycerol–Derived Liquids with Dual Functional Groups: Nonsymmetric (E/Z)–Isomeric Mixtures of 1, 3-Diether-2-Alkenes, *Chem. – Eur. J.*, 2025, e01406.
38 Z. Sekhavat Pour, P. S. Shinde, J. Wang, C. Woods, S. Taylor, S. Chatterjee and J. E. Bara, 1, 3-Diether-2-Methacrylates with Glycerol Skeletons: Tunable Resins for Stereolithography 3D Printing, *Polym. Chem.*, 2025, **16**, 2840–2850.
39 L. Zakrzewski, Y. Kim, Y. Song, C. Y. Ryu, C. Bae and C. R. Picu, Interplay of photopolymerization and phase separation kinetics and the resulting structure-property relationship of photocurable resins, *Polymer*, 2023, **280**, 126032.
40 Y. Kawagoe, G. Kikugawa, K. Shirasu, Y. Kinugawa and T. Okabe, Dissipative particle dynamics simulation for reaction-induced phase separation of thermoset/thermoplastic blends, *J. Phys. Chem. B*, 2024, **128**(8), 2018–2027.
41 S. J. Curley and C. R. Szczepanski, Applying Hansen Solubility Parameters to Dynamically Reacting Systems– A Case Study of Photopolymerization Induced Phase Separation, *ACS Mater. Lett.*, 2025, **7**(9), 3206–3212.
42 E. Hasa, T. Y. Lee and C. A. Guymon, Controlling phase separated domains in UV-curable formulations with OH-functionalized prepolymers, *Polym. Chem.*, 2022, **13**(21), 3102–3115.
43 J. Joy, K. Winkler, K. Joseph, S. Anas and S. Thomas, Epoxy/methyl methacrylate acrylonitrile butadiene styrene (MABS) copolymer blends: Reaction-induced viscoelastic phase separation, morphology development and mechanical properties, *New J. Chem.*, 2019, **43**(23), 9216–9225.
44 Z. Xu, D. Sun, J. Xu, R. Yang, J. D. Russell and G. Liu, Progress and challenges in polystyrene recycling and upcycling, *ChemSusChem*, 2024, **17**(17), e202400474.
45 Z. Sekhavat Pour, P. S. Shinde and J. E. Bara, Upcycling of Polystyrene Waste to Poly (ionic liquid) Materials, *ACS Appl. Polym. Mater.*, 2024, **6**(23), 14309–14319.
46 J.-J. Tzeng, T.-S. Yang, W.-F. Lee, H. Chen and H.-M. Chang, Mechanical properties and biocompatibility of urethane acrylate-based 3D-printed denture base resin, *Polymers*, 2021, **13**(5), 822.
47 M. Diamantopoulou, N. Karathanasopoulos and D. Mohr, Stress-strain response of polymers made through two-photon lithography: Micro-scale experiments and neural network modeling, *Addit. Manuf.*, 2021, **47**, 102266.
48 S. Venkatram, C. Kim, A. Chandrasekaran and R. Ramprasad, Critical assessment of the Hildebrand and Hansen solubility parameters for polymers, *J. Chem. Inf. Model.*, 2019, **59**(10), 4188–4194.
49 V. S. Voet, T. Strating, G. H. Schnelting, P. Dijkstra, M. Tietema, J. Xu, A. J. Woortman, K. Loos, J. Jager and R. Folkersma, Biobased acrylate photocurable resin formulation for stereolithography 3D printing, *ACS Omega*, 2018, **3**(2), 1403–1408.
50 Z. Weng, Y. Zhou, W. Lin, T. Senthil and L. Wu, Structure-property relationship of nano enhanced stereolithography resin for desktop SLA 3D printer, *Composites, Part A*, 2016, **88**, 234–242.
51 X. Kong, M. Dong, M. Du, J. Qian, J. Yin, Q. Zheng and Z. L. Wu, Recent Progress in 3D Printing of Polymer Materials as Soft Actuators and Robots, *Chem Bio Eng.*, 2024, **1**(4), 312–329.
52 S.-A. Xu and C.-M. Chan, Polystyrene/high density polyethylene blends compatibilized by a tri-block copolymer I. Properties and morphology, *Polym. J.*, 1998, **30**(7), 552–558.
53 C. Chuai, K. Almdal, I. Johannsen and J. Lyngaae-Jørgensen, Miscibility evolution of polycarbonate/polystyrene blends during compounding, *Polym. Eng. Sci.*, 2002, **42**(5), 961–968.
54 Y. Komori, A. Taniguchi, H. Shibata, S. Goto and H. Saito, Partial miscibility and concentration distribution of two-phase blends of crosslinked NBR and PVC, *Polymers*, 2023, **15**(6), 1383.
55 F. P. La Mantia, M. Morreale, L. Botta, M. C. Mistretta, M. Ceraulo and R. Scaffaro, Degradation of polymer blends: A brief review, *Polym. Degrad. Stab.*, 2017, **145**, 79–92.
56 N. Netsch, L. Schröder, M. Zeller, I. Neugber, D. Merz, C. O. Klein, S. Tavakkol and D. Stapf, Thermogravimetric study on thermal degradation kinetics and polymer interactions in mixed thermoplastics, *J. Therm. Anal. Calorim.*, 2025, **150**(1), 211–229.
57 R. Tuffi, S. D'abramo, L. Cafiero, E. Trinca and S. V. Ciprioti, Thermal behavior and pyrolytic degradation

kinetics of polymeric mixtures from waste packaging plastics, *eXPRESS Polym. Lett.*, 2018, **12**(1), 82–99.
58 U. V. Nikulova and A. E. Chalykh, Phase Equilibrium and Interdiffusion in Blends of Polystyrene with Polyacrylates, *Polymers*, 2021, **13**(14), 2283.
59 M. Grosso and P. L. Maffettone, Fourier transform rheology: A new tool to characterize material properties, *Fourier Transforms: New Anal. Approaches FTIR Strategies*, 2011, **285**, 1–20.
60 A. Thirugnanasamabandam, R. Nallamuthu, M. Renjit and C. L. Gnanasagaran, 3D–printed PLA/PMMA polymer composites: A consolidated feasible characteristic investigation for dental applications, *Polym. Eng. Sci.*, 2024, **64**(9), 4019–4031.